Laser and Particle Beams (2014), *32*, 233–241.
© Cambridge University Press, 2014 0263-0346/14 $20.00
doi:10.1017/S0263034614000044

Characterization of laser-driven electron and photon beams using the Monte Carlo code FLUKA

F. FIORINI,[1] D. NEELY,[2] R.J. CLARKE,[2] AND S. GREEN[3]

[1]Gray Institute for Radiation Oncology and Biology, Department of Oncology, University of Oxford, Oxford, United Kingdom
[2]Central Laser Facility, STFC RAL, Oxfordshire, United Kingdom
[3]Hall-Edwards Radiotherapy Research Group, Department of Medical Physics, University Hospital Birmingham NHS Trust, Birmingham, United Kingdom

(RECEIVED 29 October 2013; ACCEPTED 13 November 2013)

Abstract

We present a new simulation method to predict the maximum possible yield of X-rays produced by electron beams accelerated by petawatt lasers irradiating thick solid targets. The novelty of the method lies in the simulation of the electron refiluxing inside the target implemented with the Monte Carlo code Fluka. The mechanism uses initial theoretical electron spectra, cold targets and refiluxing electrons forced to re-enter the target iteratively. Collective beam plasma effects are not implemented in the simulation. Considering the maximum X-ray yield obtained for a given target thickness and material, the relationship between the irradiated target mass thickness and the initial electron temperature is determined, as well as the effect of the refiluxing on X-ray yield. The presented study helps to understand which electron temperature should be produced in order to generate a particular X-ray beam. Several applications, including medical and security imaging, could benefit from laser generated X-ray beams, so an understanding of the material and the thickness maximizing the yields or producing particular spectral characteristics is necessary. On the other more immediate hand, if this study is experimentally reproduced at the beginning of an experiment in which there is an interest in laser-driven electron and/or photon beams, it can be used to check that the electron temperature is as expected according to the laser parameters.

Keywords: Electron beam temperature; Electron refiluxing; Laser-driven electron beams; Laser-driven X-ray beams; Monte Carlo Fluka simulations

1. INTRODUCTION

In a typical laser-particle acceleration experiment (Daido *et al.*, 2012), a high power laser pulse (intensity above 10^{18} W/cm^2) is focused onto a solid or gaseous target. The main pulse is usually preceded by a pedestal and several pre-pulses which can create plasma on the surface of the target. The pedestal is due to incoherent spontaneous emissions of the media generating the pulse, amplified mainly in the pre-amplification stage, and the pre-pulses, of the duration of picoseconds, are due to unwanted reflections of the bunch. When the main pulse arrives, it interacts with this plasma and a population of hot electrons with a Maxwellian-type distribution is generated. These electrons can traverse the target and build up a high electrostatic field, up to the order of TV/m, capable of accelerating particles on the rear surface of the target. Photons, mainly due to bremsstrahlung and characteriztic line emission, are also produced as the electron beam crosses the target.

Supposing that the target is irradiated normal to the surface, when the main pulse arrives on the plasma created by the pre-pulse, the electrons feel the strong electric field, $\vec{E}$, carried by the pulse and start to oscillate on the target surface with velocity $\vec{v}$ parallel to $\vec{E}$ (and opposite sense). These moving electrons feel also the magnetic field, $\vec{B}$, carried by the pulse, so that a Lorentz force starts acting. Being $\vec{F} = -e\vec{v} \times \vec{B}$, the electrons start drifting across the target parallel to the laser direction ($\vec{k_L}$). The combined force of the electric and magnetic field of the laser is called *ponderomotive force* (Eliezer, 2002) and its direction does not depend on the charge of the accelerated particle. Wilks (1992) found that due to the ponderomotive force the electrons spectrum

Address correspondence and reprint requests to: F. Fiorini, Gray Institute for Radiation Oncology and Biology, Department of Oncology, University of Oxford, Roosevelt Drive, Oxford, OX3 7DQ, UK. E-mail: francesca.fiorini@oncology.ox.ac.uk or francesca.fiorini83@gmail.com

https://doi.org/10.1017/S0263034614000044 Published online by Cambridge University Press

resembles a relativistic Maxwellian distribution with an effective temperature, T_{PM}, given by Eq. (1):

$$k_B T_{PM} \simeq m_e c^2 \left[\left(1 + \frac{I\lambda^2}{1.37 \times 10^{18}} \right)^{1/2} - 1 \right], \quad (1)$$

where $k_B T_{PM}$ is measured in MeV, m_e is the electron mass in MeV/c^2, I is the laser intensity in W/cm^2 and λ its wavelength in μm. Therefore, this cloud of hot electrons is pushed forward creating a strong electric field (up to the order of TV/m). The build up of such high current must be opposed by an inductively or electrostatically generated electric field which acts to confine the fast electrons near the surface of the target, or else the background thermal plasma must supply a balancing return current. Upon reaching the rear surface of the target some of the hottest electrons escape creating a residual charge build up on the target which acts to stop further electrons from escaping. The majority of electrons are therefore "reflected" back into the target. A similar situation later occurs at the front of the target: most of the electrons return to the front surface and some escape. This phenomenon is called electron refluxing (Bell *et al.*, 1997). The percentage of refluxing electrons and the number of refluxes change with the target and laser beam characteristics (Myatt *et al.*, 2007; Quinn *et al.*, 2011).

If the target is extremely thin (tens of nn), since the accelerated electrons are very energetic, the target will effectively be transparent for them because the energy loss will be negligible: the electron cloud will reach the back of the target where it will ionize and accelerate protons from the contaminant layer on the back of the target (Wilks *et al.*, 2001; Fiorini *et al.*, 2011). If the target is not extremely thin, it will not appear transparent to the electron cloud and during its multiple paths inside the target, decreasing its energy, will generate X-rays, mostly bremsstrahlung and shell emissions, but also gammas from photo-nuclear reactions and pair production if the electron energy is sufficiently high. In this situation proton and ion acceleration can be drastically reduced.

If the target is not irradiated perpendicularly, the electric field, and in particular the component parallel to the plasma cloud, will still act as the starter of the ponderomotive force accelerating the electrons along the laser axis, but also *resonance absorption* will become relevant. In this case, when the electron plasma frequency is equal to the laser frequency (Freidberg *et al.*, 1972), the laser drives a plasma wave at the critical density surface in a plasma density gradient (Kruer & Dawson, 1989), i.e., along the normal to the target. Beg *et al.* (1997) explained that the temperature of the electrons accelerated by resonance absorption is given by Eq. (2):

$$k_B T_{res} \simeq 0.24 \left(\frac{I\lambda^2}{10^{18}} \right)^{1/3}, \quad (2)$$

where $k_B T_{res}$ is the effective electron energy of the Maxwellian spectrum measured in MeV, I is the laser intensity in W/cm^2 and λ its wavelength in μm.

As reported by Cho *et al.* (2009), for a solid target irradiated at 45°, these two mechanisms can occur together causing the acceleration of two separate beams which can be detected simultaneously. Cho reports that the beam due to resonance absorption, which shows the characteristic laser frequency, was almost an order of magnitude more intense than the beam accelerated by the ponderomotive force. It also exhibited a greater divergence. At the same time the temperatures of the two beams were estimated to be different and in good agreement with those expected using Eqs. (1) and (2).

Another similar situation is documented by Santala *et al.* (2000), who detected the X-rays emitted from Ta targets irradiated at 45° by the Vulcan laser ($I \sim 2 \times 10^{19}$ W/cm^2, energy incident on target 2050 J and main pulseduration 11.5 ps). They found that depending on the pre-plasma scale length, the two electron beams, and so the X-ray beams created by them, could even merge together generating a single beam exiting the target. In particular at plasma scale lengths closer to the laser wavelength, resonance absorption was found to be the dominant mechanism and so the electrons were mainly accelerated along the target normal. At large plasma scale lengths the ponderomotive force became the main mechanism and the electrons were mainly accelerated along the laser axis. Hence, when a target is irradiated non perpendicularly, the electrons are accelerated by two different mechanisms and therefore they and the secondary accelerated particles (photons, protons and ions) will exhibit different energetic spectra.

At present, simulation programs capable of predicting exactly what happens in matter when a laser pulse hits a target are few. Experiments at high intensity have been simulated using collisionless particle-in-cell (PIC) codes. They are called collisionless because they assume that the "hot" electrons generated by the laser beam interacting with the target have a high energy and can travel through the target (generally with thicknesses of the order of μm or less) without interactions. Collisionless PIC simulation codes can therefore be an approximate source of comparison with real experiments for high MeV electron beams accelerated in very thin targets, where the real energy loss is negligible. They become unsatisfactory in the case of thick targets where the beam energy lost crossing the target is not negligible. At the same time, Monte Carlo codes used in particle and nuclear physics, are not able yet to simulate laser-matter or laser-plasma interactions, but they are well capable of simulating "cold" electron beams moving inside matter.

In advance of a simulation code able to reproduce laser-matter as well as particle-matter interactions, we have implemented a simulation study of a simplified electron refluxing scheme in several different thick targets to investigate the X-ray production, which would be otherwise impossible using collisionless PIC codes. Theoretical hot electron spectra have been involved and changing material and thickness of the perpendicularly irradiated

https://doi.org/10.1017/S0263034614000044 Published online by Cambridge University Press

targets, it has been possible to obtain indications of relative photon/electron fields emerging from the targets and the combinations kT-material-thickness giving the maximum photon yield.

2. SIMULATION IMPLEMENTATION OF ELECTRON REFLUX

The simulations presented in this work have been performed using the Monte Carlo code Fluka (Battistoni *et al.*, 2007; Fassò *et al.*, 2005). Fluka is not meant to simulate the reactions produced by lasers, but it can simulate the electron interactions producing the photon beam in cold matter. The reactions due to the electric field occurring in the target cannot be simulated using Fluka, so the following approach was taken: (1) since the laser interacts with a plasma created on a very thin layer (few micrometers) of the target, the produced electron spectrum is only dependent on the laser characteristics and not on the target material; (2) the electron reflux is simulated by "hand". The electron beam exiting the target is forced to re-enter the target: the spectrum of the outgoing electrons is saved and while X% of the most energetic electrons can escape, (100-X)% of them are forced to re-enter the target. The chosen X for this study was mainly 10 (Nilson *et al.*, 2012); (3) each refluxing electron is reinserted in the target from the same point where it escaped and its direction cosines are inverted (Quinn *et al.*, 2011); (4) second and third points above are repeated until the number of exiting electrons at the end of one of the reflux processes is null; (5) the spectra of the photons emitted forward at the end of each reflux process is saved. The sum of all the "forward" photon spectra is the result of this simulation study for each used target. Figure 1 show a schematic view of the simulation approach. In Fiorini (2012), a very detailed

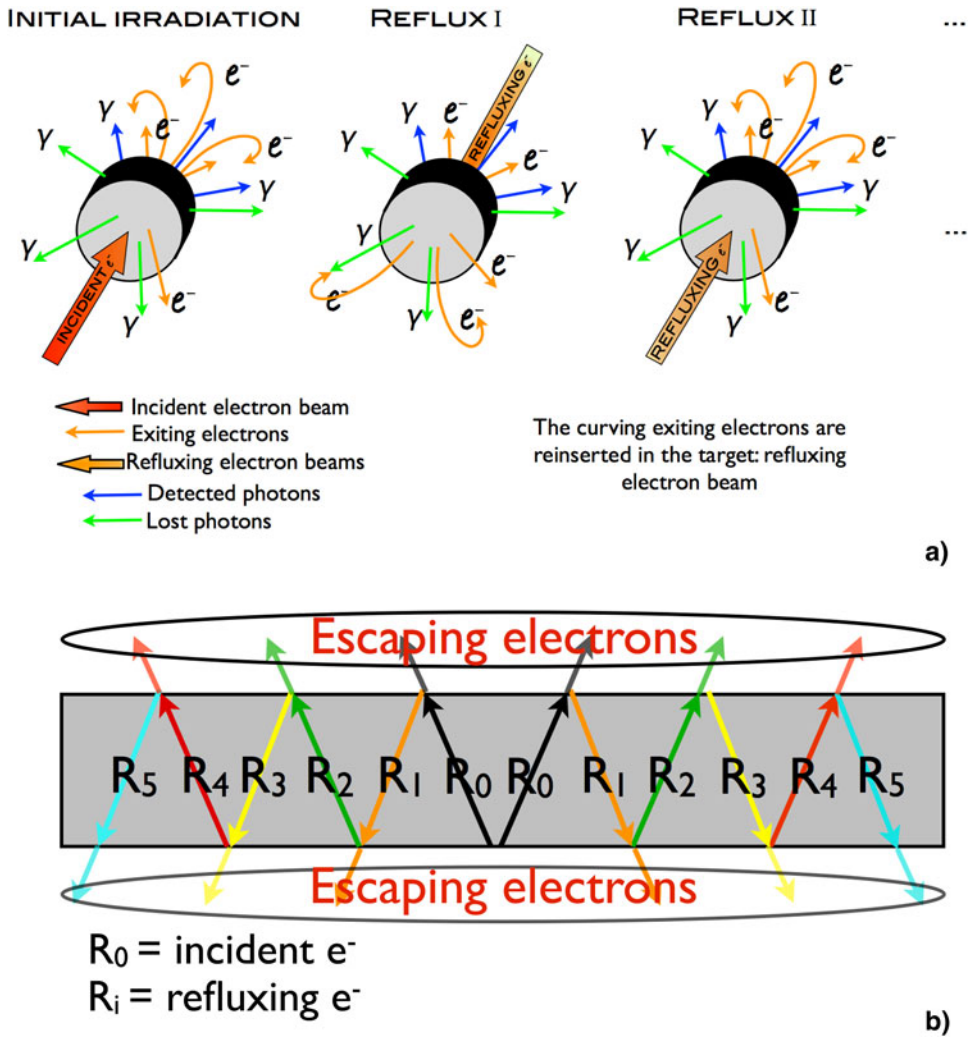


Fig. 1. (Color online) Schematic view of simulation approach of the laser-driven electron and X-ray beams. (**a**) The refluxing electrons, 90% of the exiting electrons with lower energy (curving orange arrows), are reinserted with their energy in the target as many times as needed to stop all of them in the target. The photon spectra are saved only for the photons emitted forward (blue arrows) where one can expect real detectors are placed. (**b**) The refluxing electrons are reinserted from the same point where they exited the target and their direction cosines on *X*, *Y*, and *Z* axes are inverted.

https://doi.org/10.1017/S0263034614000044 Published online by Cambridge University Press

explanation of the cards and user routines used in Fluka to perform these simulations is reported. However, some basic information is presented here in order to fully explain the implementation of the input file: CALORIME was the chosen default, the MULSOP card was used for the lowest electron temperatures to activate the single scattering given the fact that Molière multiple scattering model becomes unreliable below 20–30 keV, and the transport and production threshold of electromagnetic particles were set to 10 keV.

The initial electron spectrum follows a quasi-Maxwellian distribution. The distributions reported in literature to describe the same process are several: $dN_e/dE = E^2\exp(-E/k_BT)$ (Ledingham & Galster, 2010), $dN_e/dE = E\exp(-E/k_BT)$ (Galy *et al.*, 2007), $dN_e/dE = \sqrt{E}\exp(-E/k_BT)$ (Perry *et al.*, 1999), $dN_e/dE = \exp(-E/k_BT)$ (Chen & Wilks, 2005), with N_e the number of electrons and E their energy. The only consistency among them is the term in k_BT, taken from the ponderomotive acceleration or resonance absorption theory, but in none of the published studies the initial electron beam was directly detected, so the best equation to use for the initial spectrum is unknown. As a result of this ambiguity in the initial spectrum, some authors saw the expected k_BT to be respected, while some others did not.

In this study we decided to use $dN_e/dE = E^2\exp(-E/k_BT)$ (Ledingham & Galster, 2010), which for simplicity from now will be identified as (E^2exp). The hot temperature (k_BT) depends on the intensity and on the wavelength of the main laser pulse and on the acting force. In particular, in the initial modelling presented here, only perpendicularly irradiated targets are considered, so that the ponderomotive force should be the only acting force. However, since the photon yield results are expressed as a function of k_BT and not of the laser intensity, the reflux mechanism employed in this study is still valid also in the case where the resonance absorption is the main acting force. In fact, the main practical differences between the two forces are in the temperature of the accelerated electron beam and in its direction. Considering several possible k_BT and detecting all the photons emitted forward, this study can well represent the case when the two forces are acting separately, creating two different and separable electron beams, or when one of the two acts to a greatest degree. In the case where the two forces act together in the target generating a single out-coming beam, the user will need to combine the results of two different temperatures, but the correct percentage of the acting forces must be known. For this same reason, in the simulations of this modelling study the initial electron beam propagates into the target without any initial divergence: the divergence is seen to be a parameter dependent on the main acting force (Cho *et al.*, 2009) on the laser intensity (Norreys *et al.*, 2009) and on the plasma effects (Quinn *et al.*, 2011; Gray *et al.*, 2011; Coury *et al.*, 2012).

In order to define the energy of each particle generated by Fluka, one of the possible ways is inverting the statistical equation of the spectrum, so that instead of N as a function of E, one has E as a function of N (with N the number of particles and E their energy). In our particular case, it is not possible to invert the functions of the distribution, so gamma distributions are used. A random variable x is gamma-distributed with scale θ and shape n if its distribution is denoted by the Eq. (3):

$$\Gamma(n, \theta) = \int_0^\infty x^{n-1}e^{-x/\theta}dx, \tag{3}$$

with $x \geq 0$ and $n, \theta > 0$. In the case of (E^2exp), $n - 1$ is 2, so that (E^2exp) = $\Gamma(3, k_BT)$. Given the properties of the gamma function, it follows that $\Gamma(3, k_BT)$ can be rewritten as in Eq. (4):

$$F^{-1}(\Gamma(3, k_BT)) = -k_BT(\ln(N_1) + \ln(N_2) + \ln(N_3)), \tag{4}$$

with N_1 ,N_2 and N_3 independent variables uniformly distributed on (0,1]. Eq. (4) has been used in the Fluka *source* routine to generate the initial electron spectra.

Targets made of different materials, covering a range of Z (or Z_{eff}) and all known to have been used experimentally, and with different thicknesses were simulated: Au, Ta, Cu, SiO_2, and PMMA. This selection was used to determine which thickness of each material maximized the number of produced X-rays and to compare the produced X-ray spectra.

3. SIMULATION RESULTS

For each set of simulation (including the sub-simulation of each single refluxing beam), the number of produced photons was saved and their spectrum was plotted. By dividing the number of photons by the number of initial electrons the yield of the photons emitted forward was calculated for each target thickness and material and for each initial k_BT.

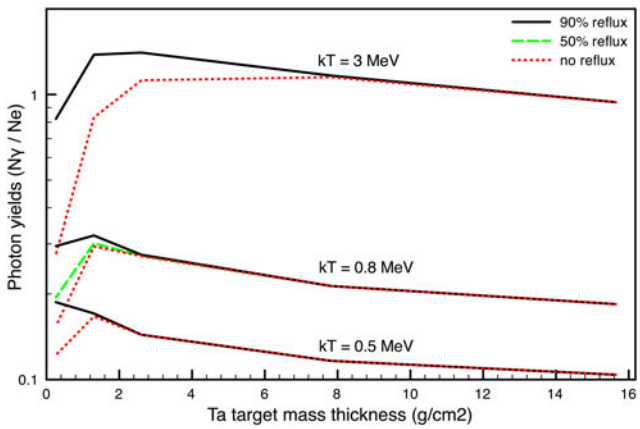


Fig. 2. (Color online) Simulated photon yields (number of photons detected forward in 2π normalised by the number of initial simulated electrons) with and without reflux for (E^2exp) distribution from Ta targets. As can be seen, at the used energies (0.5, 0.8, and 3 MeV), the photon yields are higher for the cases where 90% reflux is used and lower where no reflux is used only for the lowest thicknesses, while there are no differences for the thickest targets.

https://doi.org/10.1017/S0263034614000044 Published online by Cambridge University Press

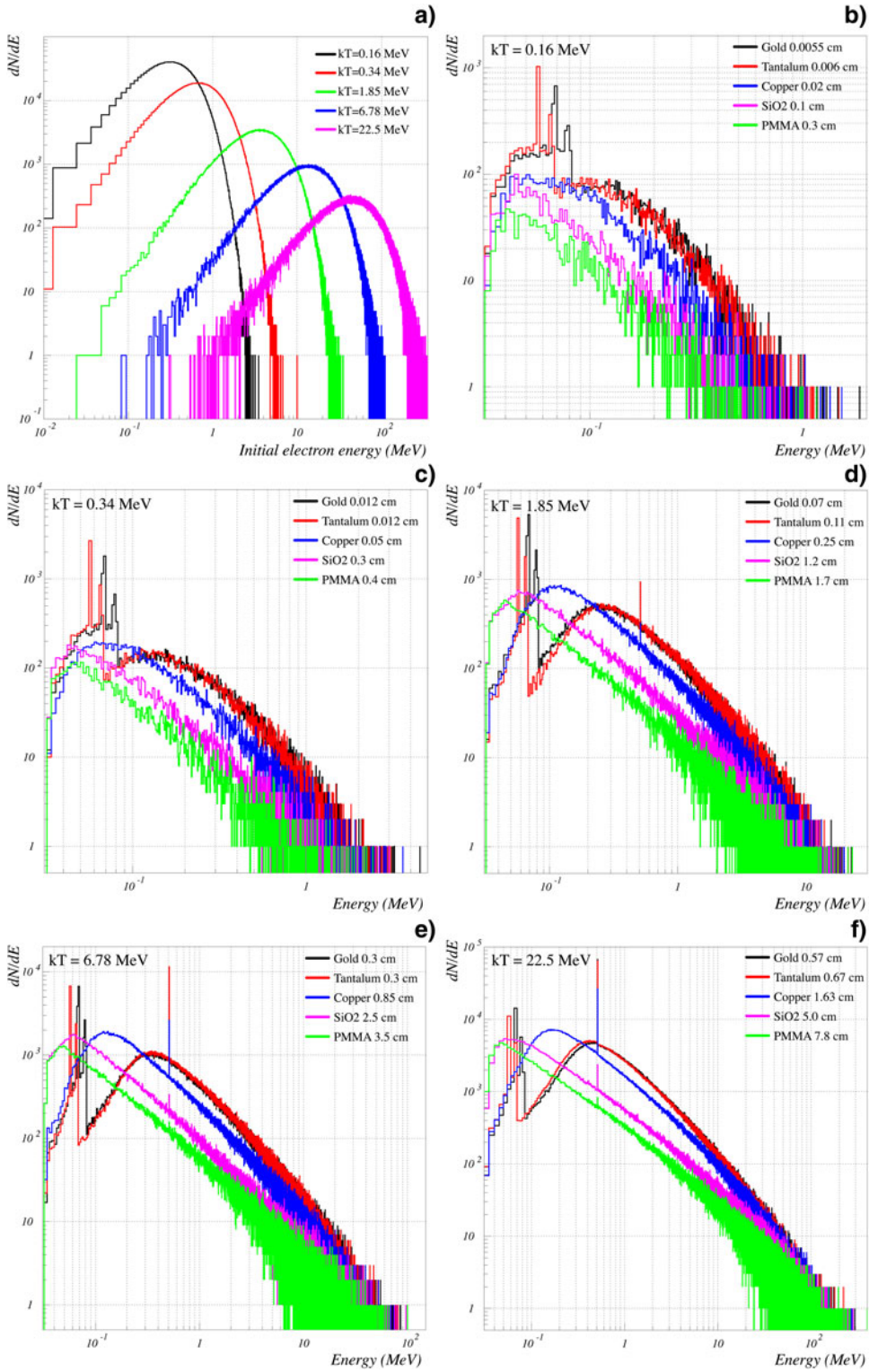


Fig. 3. (Color online) (**a**) Simulated initial electron spectra with (E^2exp) distribution. From (**b**) to (**f**) simulated spectra of the photons emitted in 2π forward from the irradiated targets for each studied initial temperature. The thicknesses of the targets shown here are those or close to those which maximise the number of forward emitted photons. The number of initial electrons for these simulations was 3×10^5.

The reflux is found to be not very effective for thick targets and low temperatures, because the majority of the electrons are stopped in the target after the initial crossing. A difference in the yields, instead, can be seen for thin targets even at low $k_B T$. Examples of photon yields for irradiated Ta targets with and without reflux are shown in Fig. 2.

https://doi.org/10.1017/S0263034614000044 Published online by Cambridge University Press

Some of the photon spectra obtained for the several k_BT simulated are shown in Fig. 3. Integrating the obtained spectra the total number of forward emitted photons can be found. The thicknesses of the targets shown in Fig. 3 are those or close to those which maximize the number of forward emitted photons for the corresponding initial electron temperature. The spectra giving the largest numbers of photons are always produced by the high Z materials (as expected from the bremsstrahlung effect) as well as the highest energy photons. The peak of the spectrum of the photons emitted from SiO_2 and PMMA targets is in both cases below 100 keV and it does not change greatly with increasing initial electron energy even for the highest studied k_BT (22.5 MeV). Moreover, for these materials, the tails in the spectra at high energies are always shorter than the tails created by the high Z targets. The K_α and K_β peaks are visible only for Au (energies between 66 and 80 keV) and Ta (energies between 55 and 67 keV) targets: this is because for the other materials the energy of K_α and K_β was lower than the transport and production energy threshold chosen for the simulations. From the graph with $k_BT = 1.85$ MeV, also annihilation photons are visible: their production is, in fact, unlikely for the other lower temperatures because of the low number of photons with energy greater than 1.02 MeV. Spectra of the escaping electrons can also be extracted from the simulations. An example for the irradiation of 1 mm Ta target and $k_BT = 2.33$ MeV is given in Fig. 4, where the forward emitted electron, positron and X-ray spectra are shown. As can be seen the tail of the simulated electron spectrum reaches energies close to 25 MeV. It also shows a spike, due to the first escaping electrons (as explained the method assumes that only 10% of the electrons exiting the target, the ones with highest energies, can escape, while the others contribute to the refluxing beam) and a peak due to other successive escaping electrons (and in particular only the odd escaping ones are detected forward, the even ones would be detected backward).

Having repeated the simulations for several target thicknesses it was possible to determine the thickness maximizing the photon yield for each simulated k_BT. Fig. 5 shows the photon yields plotted as a function of the mass thickness for each material and initial electron temperature studied. Plotting the initial electron temperatures used in the simulations as a function of the mass thicknesses giving the maximum photon yields for each material, the graph in Fig. 6 was obtained.

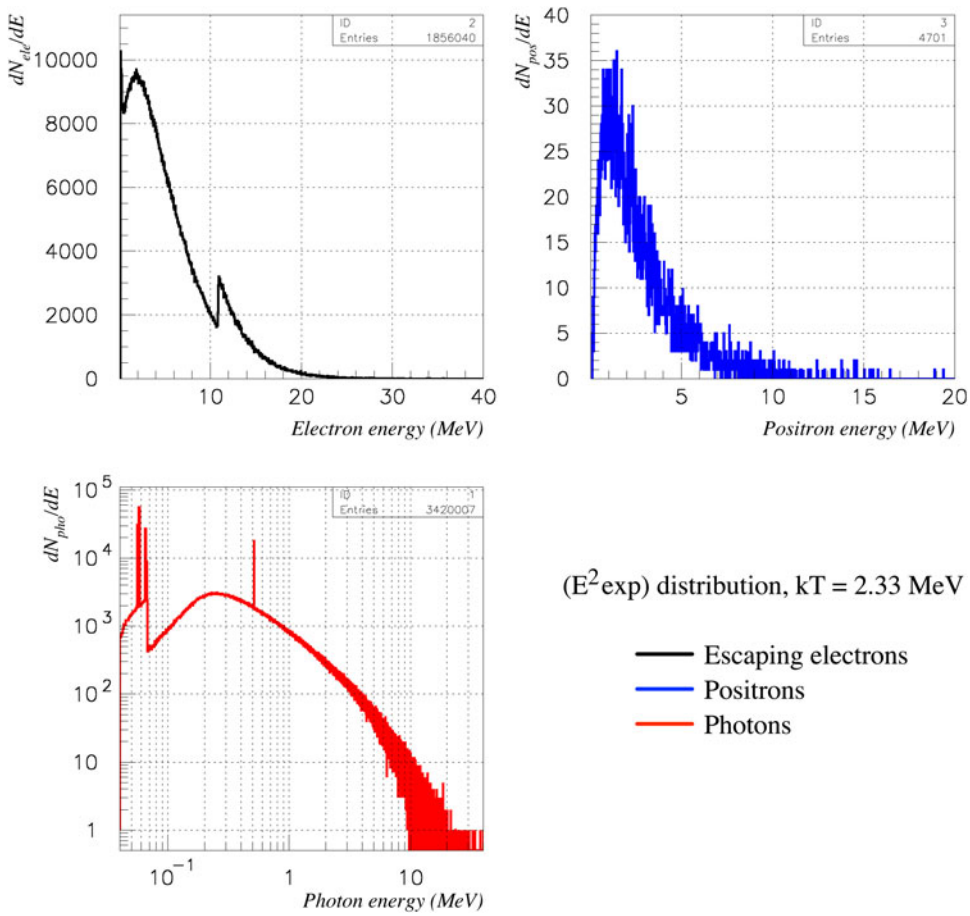


Fig. 4. (Color online) Simulated spectra of the forward (2π) emitted particles for the (E^2exp) distribution with $k_BT = 2.33$ MeV irradiating a 1 mm thick tantalum target. The number of initial electrons for these simulations was 3×10^5.

https://doi.org/10.1017/S0263034614000044 Published online by Cambridge University Press

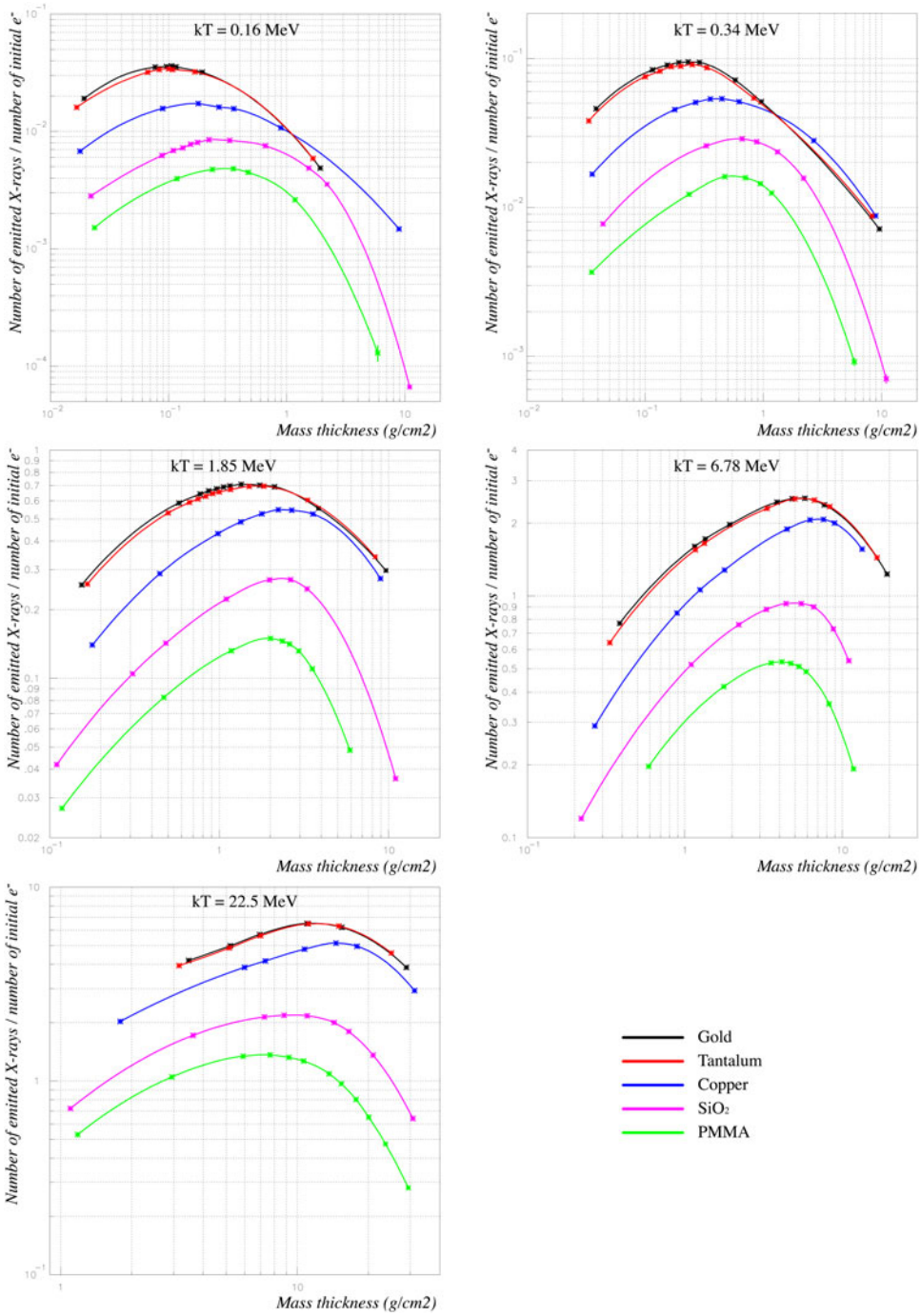


Fig. 5. (Color online) Simulated photon yields (integrated over all energies) as a function of the target mass thickness for gold, tantalum, copper, SiO_2 and PMMA for a range of initial temperatures (0.16–22.5 MeV).

4. CONCLUSIONS AND DISCUSSIONS

In order to obtain the largest photon yields, not only the material (or better, its atomic number Z or Z_{eff}) is important but also its thickness. Several applications (Nishikino *et al.*, 2009; Glinec *et al.*, 2005) can use laser generated X-ray beams and an understanding of the material and the thickness which maximize the yields or produce particular spectral characteriztics would be useful. With regard to this, the yield study described here could be used as a method to estimate the initial temperature of the laser-driven electron beam and so the maximum X-ray yields attainable by irradiating thick targets, notwithstanding the assumptions made and the fact that there are no plasma effects in the simulations. The important experimental step would be the irradiation of targets of the same material for a wide range of thicknesses. Detecting the number of photons (or even

https://doi.org/10.1017/S0263034614000044 Published online by Cambridge University Press

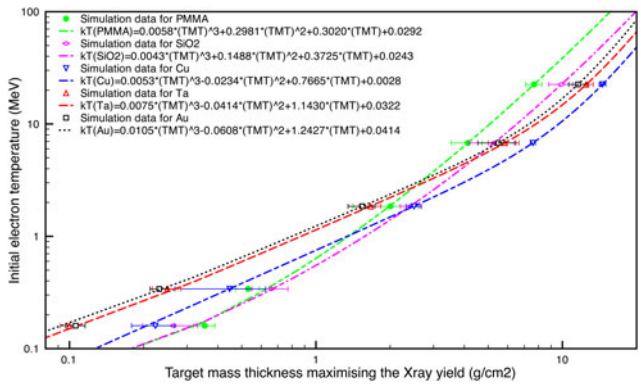


Fig. 6. (Color online) Initial electron temperature as a function of the target mass thickness giving the maximum X-ray yield integrated over all energies for each studied material. Empirical line fits provided to guide the eye.

the dose due to photons) in 2π forward, it would be possible to determine which thickness maximizes the photon yield and so, by using the curves in Fig. 6, estimate the initial electron temperature. Measuring the spectrum of the escaping electrons would also serve to estimate the initial electron temperature by comparing the experimental spectra with the simulations (graphs like those shown in Fig. 4). These tests could be implemented whenever there is an interest in using laser-driven electron and/or photon beams. In fact, they could be performed during the first day of an experiment to check that the electron energy is as expected according to the laser parameters.

With regard to the spectra in Fig. 3, it can be seen that the spectral distribution of the emitted photons varies with the material composition of the irradiated target and with the k_BT of the initial electron beam. Particular materials and laser intensities (and so k_BT) could be chosen according to the necessary characteristics of the X-ray beam. For example, low intensity lasers and low Z_{eff} targets, such as PMMA or SiO_2, could be suitable for transmission medical radiography, since the energy of the created photons would be likely to generate good contrast under clinical conditions. Conversely, tomography of objects generally requires higher intensity beams, so that high power lasers could be useful for security applications ranging from high speed imaging of objects in motion to airport or container imaging.

As mentioned earlier, in this study the divergence of the initial electron beam was not considered as it has been seen to be dependent on the main acting force, the laser intensity and plasma effects (Quinn *et al.*, 2011; Cho *et al.*, 2009; Norreys *et al.*, 2009; Gray *et al.*, 2011; Coury *et al.*, 2012). However in the case of imaging, knowing the divergence of the produced photon beams is essential, since it is critical for determining the focal spot size of any future imaging system. This means that experimental studies are required to improve knowledge of the initial electron beam divergence (and its dependence on the laser parameters) in order to be able to correctly implement it in the Monte Carlo simulations and so produce more realistic directional photon beams.

ACKNOWLEDGEMENT

The presented work was funded by the LIBRA consortium grant from EPSRC, grant no EP/E035728/1.

REFERENCES

Battistoni, G, Muraro, S., Sala, P.R., Cerutti, F., Ferrari, A., Roesler, S., Fassò, A. & Ranft, J. (2007). The FLUKA code: Description and benchmarking. *AIP Confer. Proc.* **896**, 31–49.

Beg, F.N., Bell, A.R., Dangor, A.E., Danson, C.N., Fews, A.P., Glinsky, M.E., Hammel, B.A., Lee, P., Norreys, P.A. & Tatarakis, M. (1997). A study of picosecond laser-solid interactions up to 10^{19} Wcm^{-2}. *Phys. Plasmas* **4**, 447–457.

Bell, A.R., Davies, J.R., Guerin, S. & Ruhl, H. (1997). Fast-electron transport in high-intensity short-pulse laser-solid experiments. *Plasma Phys. Contr. Fusion* **39**, 653.

Chen, H. & Wilks, S.C. (2005). Evidence of enhanced effective hot electron temperatures in ultraintense laser-solid interactions due to reflexing. *Laser Part. Beams-Pulse Power & High Energy Densities* **23**, 411–416.

Cho, B.I., Osterholz, J., Bernstein, A.C., Dyer, G.M., Karmakar, A., PUnited Kingdomhov, A. & Ditmire, T. (2009). Characterization of two distinct, simultaneous hot electron beams in intense laser-solid interactions. *Phys. Rev. E* **80**, 055402.

Coury, M., Carroll, D.C., Robinson, A.P.L., Yuan, X.H., Brenner, C.M., Burza, M., Gray, R.J., Quinn, M.N., Lancaster, K.L., Li, Y.T., et al. (2012). Influence of laser irradiated spot size on energetic electron injection and proton acceleration in foil targets. *Appl. Phys. Lett.* **100**, 074105–074105.

Daido, H., Nishiuchi, M. & Pirozhkov, A.S. (2012). Review of laser-driven ion sources and their applications. *Reports Progr. Phys.* **75**, 056401.

Eliezer, S. (2002) *The interaction of high-power lasers with plasmas*. New York: Taylor & Francis.

Fassò, A., Ferrari, A., Ranft, J. & Sala, P.R. (2005). FLUKA: a multi-particle transport code. CERN-2005-10. *INFN/TC_05/11, SLAC-R-773*.

Fiorini, F. (2012). *Experimental and computational dosimetry of laser-driven radiation beams.* PhD thesis, Birmingham:, University of Birmingham.

Fiorini, F., Kirby, D., Borghesi, M., Doria, D., Jeynes, J.C.G., Kakolee, K.F., Kar, S., Litt, S.K., Kirkby, K.J., Merchant, M.J. & Green, S. (2011). Dosimetry and spectral analysis of a radiobiological experiment using laser-driven proton beams. *Phys. Med. Biol.* **56**, 6969–6982.

Freidberg, J.P., Mitchell, R.W., Morse, R.L. & Rudsinski, L.I. (1972). Resonant absorption of laser light by plasma targets. *Phys. Rev. Lett.* **28**, 795–799.

Galy, J., Maučec, M., Hamilton, D.J., Edwards, R. & Magill, J. (2007). Bremsstrahlung production with high-intensity laser matter interactions and applications. *New J. Phys.* **9**, 23.

Glinec, Y., Faure, J., Dain, L.L., Darbon, S., Hosokai, T., Santos, J.J., Lefebvre, E., Rousseau, J.P., Burgy, F., Mercier, B., et al. (2005). High-resolution γ-ray radiography produced by a laser-plasma driven electron source. *Phys. Rev. Lett.* **94**, 25003.

Gray, R.J., Yuan, X.H., Carroll, D.C., Brenner, C.M., Coury, M., Quinn, M.N., Tresca, O., Zielbauer, B., Aurand, B., Bagnoud, V., et al. (2011). Surface transport of energetic electrons in intense picosecond laser-foil interactions. *Appl. Phys. Lett.* **99**, 171502–171502.

https://doi.org/10.1017/S0263034614000044 Published online by Cambridge University Press

Kruer, W.L. & Dawson, J.M. (1989). The physics of laser plasma interactions. *Phys. Today* **42**, 69.

Ledingham, K.W.D. & Galster, W. (2010). Laser-driven particle and photon beams and some applications. *New J. Phys.* **12**, 045005.

Myatt, J., Theobald, W., Delettrez, J.A., Stoeckl, C., Storm, M., Sangster, T.C., Maximov, A.V. & Short, R.W. (2007). High-intensity laser interactions with mass-limited solid targets and implications for fast-ignition experiments on OMEGA EP. *Phys. Plasmas* **14**, 056301.

Nilson, P.M., Davies, J.R., Theobald, W., Jaanimagi, P.A., Mileham, C., Jungquist, R.K., Stoeckl, C., Begishev, I.A., Solodov, A.A., Myatt, J.F., Zuegel, J.D., Sangster, T.C., Betti, R. & Meyerhofer, D.D. (2012). Time-resolved measurements of hot-electron equilibration dynamics in high-intensity laser interactions with thin-foil solid targets. *Phys. Rev. Lett.* **108**, 085002.

Nishikino, M., Sato, K., Ohshima, S., Hasegawa, N., Ishino, M., Kawachi, T., Okano, Y., Numasaki, H., Teshima, T. & Nishimura, H. (2009). Development of focused laser plasma x-ray beam for radiobiological applications. *Conference on Lasers and Electro-Optics/Pacific Rim*. Optical Society of America.

Norreys, P.A., Scott, R.H.H., Lancaster, K.L., Green, J.S., Robinson, A.P.L., Sherlock, M., Evans, R.G., Haines, M.G., Kar, S., Zepf, M., et al. (2009). Recent fast electron energy transport experiments relevant to fast ignition inertial fusion. *Nucl. Fusion* **49**, 104023.

Perry, M.D., Sefcik, J.A., Cowan, T., Hatchett, S., Hunt, A., Moran, M., Pennington, D., Snavely, R. & Wilks, S.C. (1999). Hard X-ray production from high intensity laser solid interactions. *Rev. Scientif. Instr.* **70**, 265.

Quinn, M.N., Yuan, X.H., Lin, X.X., Carroll, D.C., Tresca, O., Gray, R.J., Coury, M., Li, C., Li, Y.T., Brenner, C.M., et al. (2011). Refluxing of fast electrons in solid targets irradiated by intense, picosecond laser pulses. *Plasma Phys. Contr. Fusion* **53**, 025007.

Santala, M.I.K., Zepf, M., Watts, I., Beg, F.N., Clark, E., Tatarakis, M., Krushelnick, K., Dangor, A.E., McCanny, T., Spencer, I., et al. (2000). Effect of the plasma density scale length on the direction of fast electrons in relativistic laser-solid interactions. *Phys. Rev. Lett.* **84**, 1459–1462.

Wilks, S.C., Kruer, W.L., Tabak, M. & Langdon, A.B. (1992). "Absorption of ultra-intense laser pulses. *Phys. Rev. Lett.* **69**, 1383–1386.

Wilks, S.C., Langdon, A.B., Cowan, T.E., Roth, M., Singh, M., Hatchett, S., Key, M.H., Pennington, D., MacKinnon, A. & Snavely, R.A. (2001). Energetic proton generation in ultra-intense laser–solid interactions. *Phys. Plasmas* **8**, 542.

https://doi.org/10.1017/S0263034614000044 Published online by Cambridge University Press